Imaging Block Copolymer Crystallization in Real Time with the Atomic Force Microscope

Jamie K. Hobbs*,† and Richard A. Register‡

Department of Chemistry, University of Sheffield, Brook Hill, Sheffield S3 7HF, UK, and Department of Chemical Engineering, Engineering Quadrangle, Princeton University, Princeton, New Jersey 08544-5263

Received June 29, 2005; Revised Manuscript Received November 21, 2005

ABSTRACT: The crystallization of two diblock copolymers, one forming a cylindrical mesophase and the other a spherical mesophase in which the crystallizable unit, polyethylene, is the minority component, has been followed in situ using high-temperature atomic force microscopy. Contrast is obtained between the crystallizable and noncrystallizable microdomains in the melt as well as between the melt and the crystalline material, allowing the influence of the melt structure on crystallization to be observed in real time. In both cases the mesophase structure is destroyed by crystallization, but its influence over the growth dynamics is followed. In the cylinder former, transport of material to the crystal growth front is found to occur primarily by diffusion, rather than by flow, leaving the melt structure unperturbed. Crystal growth rates vary considerably between individual crystallites, with more rapid growth along existing ethylene-rich domains. Melting occurs randomly along the crystallites, leading to their breakup into small blocks. In the sphere former crystallization leads to a densely branched seaweed structure, the morphology controlled by the directionally varying diffusion rate between the ethylene-rich spherical domains. On increasing supercooling the extent to which the spherical melt structure controls the crystal morphology increases, with crystal growth directions dominated by sphere−sphere nearest-neighbor angles.

Introduction

Over recent years the crystallization behavior of block copolymers with one crystallizable block, from the phase-separated melt, has been extensively studied.[1−5] By careful control over molecular length and temperature, it is possible to tune the behavior of the melt so as to give varying strengths of phase segregation and hence to control a range of behaviors from pure "break-out", where the crystallization effectively ignores the existing melt structure, to complete confinement, where individual crystallites are completely confined within preexisting nanometric domains.[1−3] These studies have not only led to a greater understanding of how block copolymers behave but also provided many insights into the crystallization behavior of homopolymers, with the ability to control domain size being a particularly powerful tool.[4−6]

Although the general scheme of break-out to confinement is well documented, the subtleties of behavior have not been extensively explored, and intriguing questions remain as to the precise impact of the melt on the trajectory of a growing crystal and the interrelation between growing crystals. Also, in some cases, it has not been possible to define the morphology during growth, as ex situ observation by TEM can be misleading, while the length scales of the structures are not observable by optical microscopy.

Over recent years, AFM has become a useful tool for studying the crystallization[7−11] and melting[12,13] behavior of polymers in situ, in real time, with nanometer resolution. The technique has already been applied to block copolymers with remarkable success, allowing direct visualization of the reorganization of the phase-separated melt,[14,15] as well as of crystallization in both spherical[4] and cylindrical domains.[16] Fortuitously, in many cases it is possible to obtain contrast both between the two components of the melt (i.e., between areas rich in each polymer block) and between those two components and the crystalline phase of one component. In this article we exploit this imaging capability to study, at elevated temperature and in real time, the crystallization of two diblock copolymers, one of which forms spheres of crystallizable material in a matrix of uncrystallizable material and another which forms cylinders of crystallizable material. The study was carried out on relatively thick films (>500 nm, so >10 microdomain layers) so that interactions with the substrate do not considerably affect the melt microdomain structure, and in the range of temperatures where crystallization is not completely templated by the existing melt structure, but where segregation between the unlike blocks still exerts a substantial influence on the course of crystallization.

Experimental Method

Two diblock copolymers were used, both containing hydrogenated high-1,4-polybutadiene ("polyethylene") as the crystallizable minority block and each having an amorphous majority block which is above its glass transition at the crystallization temperatures examined. The synthesis and characterization of hydrogenated poly(high-1,4-butadiene)-*b*-poly(styrene-*r*-butadiene), denoted E/SEB, are described in ref 3. The sample used in the current study had blocks of molar mass M_n of 5 and 30 kg/mol, respectively. This material forms a spherical mesophase in the melt. The synthesis and characterization of hydrogenated poly(high-1,4-butadiene)-*b*-poly(high-3,4-isoprene), denoted E/MB, are described in ref 17. The sample used in the current study had blocks with molar mass of 17 and 45 kg/mol, respectively. This material forms a cylindrical mesophase in the melt.

Samples were melt-cast onto glass coverslips at 130 °C and thinned using a razor blade to give a film thickness of 500−1000 nm. A Veeco Dimension D3100 with a Nanoscope IIIa controller was used to obtain AFM images. Images were obtained in Tapping Mode using standard silicon cantilevers, nominal spring constant 50 N m^{-1}, with a resonant frequency of around 300 kHz. To allow high-temperature imaging, the setup previously described in ref 18 was utilized. This is a similar set up to that detailed in ref 19, in

* Corresponding author. E-mail: jamie.hobbs@sheffield.ac.uk.
† University of Sheffield.
‡ Princeton University.

10.1021/ma0514020 CCC: $33.50
Published on Web 12/21/2005

which the cantilever is insulated from the effective heat sink of the scanner through the use of a glass−air−glass sandwich, allowing the cantilever to thermally equilibrate with the sample surface. However, in this case,[18] the cantilever is driven with a magnetostrictive oscillator, maintaining the thermal isolation of the cantilever that would otherwise be broken by conductive links to a drive piezo, but removing the need for magnetically coated cantilevers. We have found that this system allows stable imaging at temperatures up to 150 °C without the need for heating of the cantilever probe. At higher temperatures too great a thermal gradient is induced between the tip and the sample, and the tip starts to act as a local cooling device, in a manner similar to that observed with other methods that do not utilize our thermal isolation approach.

Most of the presented images are "phase" images, in which contrast consists of a combination of mechanical and adhesive properties of the sample surface. The tapping force was kept to the minimum possible to maintain both control while imaging and contrast between the three different phases (two melt phases and the crystalline phase).

Results

In the systems studied, a clear phase contrast was obtained between areas of the melt rich in the two different components, despite the fact that both components are well above their glass transition temperatures. In the images shown, the MB- or SEB-rich domains are darkest, followed by the ethylene-rich domains, with the crystalline ethylene areas having the brightest contrast. Contrast in AFM phase images is primarily related to dissipative interactions between the AFM tip and the surface,[20] although variations in stiffness will lead to changes in surface contact area and hence adhesive interactions, leading to a combination of elastic and viscous influences on the final image. The plateau modulus of the ethylene domains in our sample (these are ethylene-*co*-butene with two ethyl branches per 100 backbone carbons) is given in ref 21 as 2.2 MPa and for MB as ∼0.35 MPa; we estimate a plateau modulus of around 0.4−0.5 MPa for SEB (taken from the 0.78 MPa value for SEB with 40% styrene[22] and the 0.20 MPa value for pure polystyrene[21]). This leads to a 5−6× modulus contrast between the two phases, which we suggest is responsible for the observed phase contrast.

Figure 1 shows images of the melt structure and coarse crystalline morphology of the two samples studied. The E/MB material forms cylindrical domains as expected, the cylinders lying primarily in the plane of the surface. MB has a significantly lower solubility parameter than E,[23,24] and consequently a lower surface energy, so the MB phase (which is also the matrix) is expected to completely cover the surface, with the E cylinders underneath; this promotes orientation of the cylinders in a plane parallel to the surface. On crystallization, radial aggregates are formed although the extent of branching is insufficient to form a spherulitic texture. The E/SEB material forms spherical domains as can be seen from Figure 1c. We have not carried out an extensive analysis of the "crystal" structure of the spherical melt as the lattice such as it is does not appear well ordered, with a very high level of defects. However, the most recurrent structure is an oblique lattice with $a = b$ at an angle of around 110°. This angle corresponds to the (110) plane of a body-centered-cubic structure (bcc is the known bulk structure of these sphere-forming materials[3]). As this is the most densely packed bcc surface, and is quite close to a hexagonal packing, it is not surprising that this plane is seen at the surface. The high level of defects within the structure most probably occurs because of frustration between the (110) bcc structure and a fully hexagonal reconstruction at the surface (films only one[26] or two[27] microdomains thick are known to be hexagonal). On crystallization, a "seaweed" morphology is formed, as can be seen from Figure 1d.

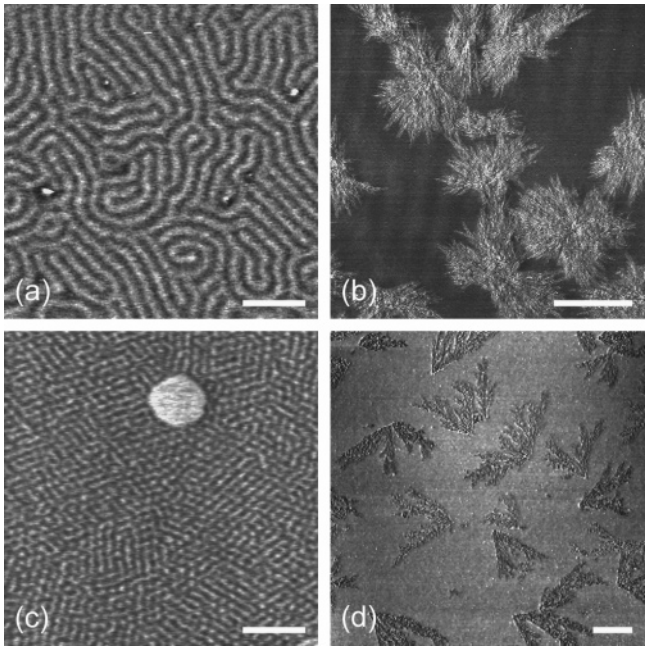

Figure 1. (a) An AFM phase image showing the melt microdomain structure in E/MB, collected at 130 °C. Black to white represents a variation in phase of 3°. The scale bar represents 200 nm. (b) An AFM phase image showing a partially crystallized film of E/MB taken during growth at 95 °C. Black to white represents a variation in phase of 5°. The scale bar represents 5 μm. (c) An AFM phase image showing the melt microdomain structure in E/SEB, collected at 90 °C. Black to white represents a variation in phase of 10°. The scale bar represents 200 nm. (d) An AFM phase image showing a partially crystallized film of E/SEB taken during growth at 85 °C. Black to white represents a variation in phase of 5°. The scale bar represents 5 μm.

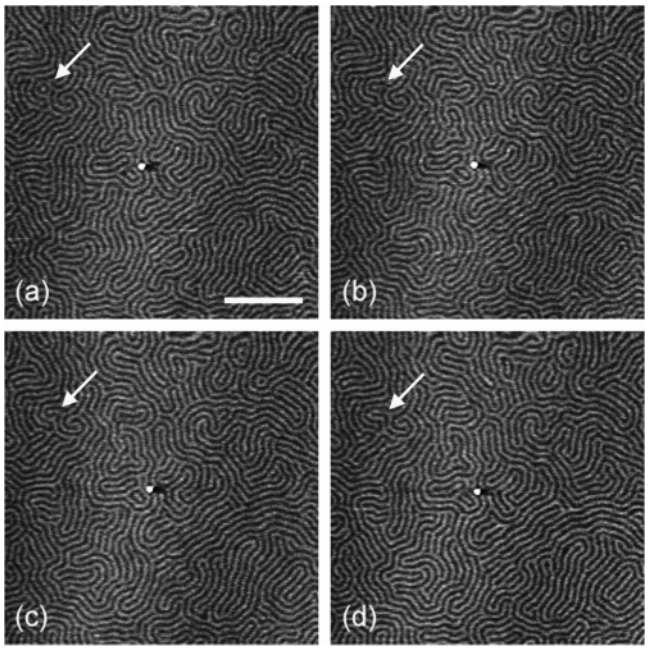

Figure 2. A series of AFM phase images showing the gradual reorganization of the E/MB melt structure at 130 °C. The white spot in the center of each image is a stationary piece of dirt that was used as a marker. The arrow indicates a region in which the cylinders are changing conformation. (a) Taken at 0 s, (b) taken at 133 s, (c) taken at 267 s, and (d) taken at 333 s, each image collected in 63 s. Black to white represents a change in phase of 3°. The scale bar represents 500 nm.

Figure 2 shows a series of AFM micrographs taken at 130 °C showing the cylindrical melt structure of E/MB as it slowly evolves over a period of nearly 6 min. Careful examination

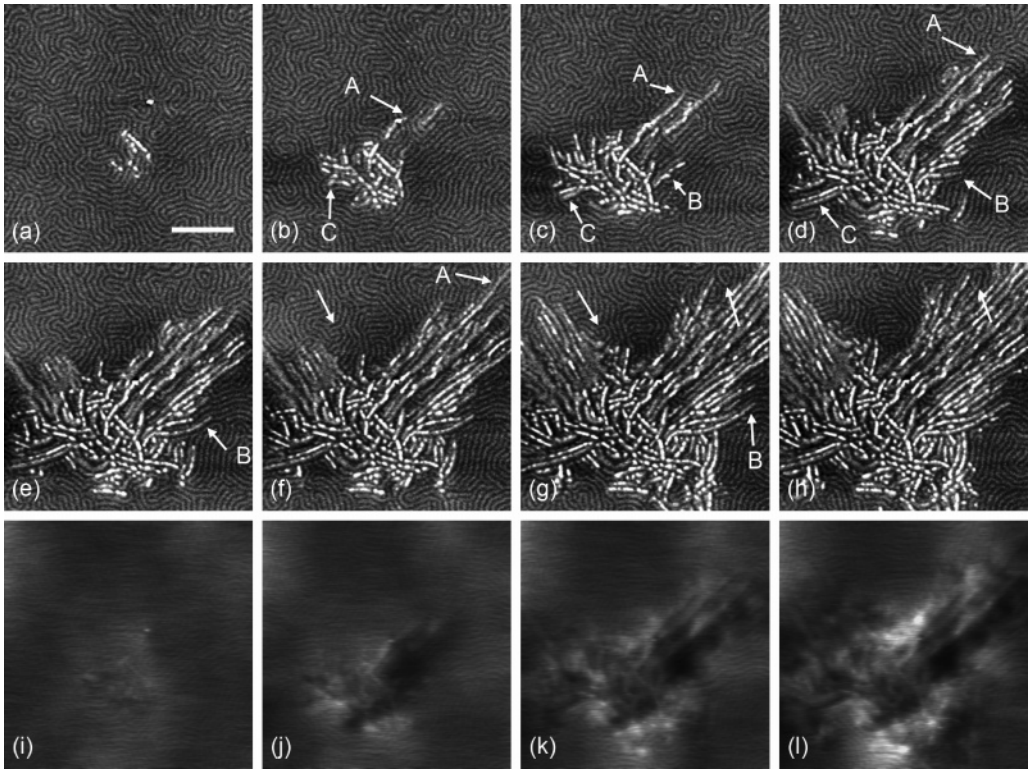

Figure 3. A series of AFM images showing the crystallization of the ethylene domains in E/MB at 95 °C. A, B, and C indicate crystallites referred to in the text. The unlabeled arrows indicate regions that can be seen to reorganize subtly just prior to crystallization. Images a−h are phase images in which black to white represents a change in phase of 3°. Images i−l are topographic images corresponding to images a, c, e, and g, in which black to white represents a change in height of 10 nm. (a) Taken at 0 s, (b) taken at 134 s, (c) taken at 271 s, (d) taken at 466 s, (e) taken at 531 s, (f) taken at 595 s, (g) taken at 724 s, and (h) taken at 791 s, each image collected in 63 s. The scale bar represents 500 nm.

shows that there is very little change in structure over this time or indeed over the 30 min duration of the experiment. However, subtle reorganizations do occur and are marked in the figure. These tend to involve the annealing out of circles, which are most probably cylinders oriented perpendicular to the surface, and changes in the connectivity of neighboring cylinders. Large-scale reorganizations are not seen at this temperature, leading to almost complete stability of the structure at lower temperatures. Supporting Information S1 is a movie showing the full sequence of images collected during the experiment.

Figure 3 shows a series of images taken during crystallization of the ethylene component at 95 °C. Figure 3a−h shows phase images, while Figure 3i−l shows topographic images corresponding to alternate phase images. In the particular series of data shown here, the crystal structure has started to grow from close to the center of the area being imaged. Two different growth behaviors are seen: growth that is primarily constrained within cylinders, characterized by the sporadic appearance of new growth apparently unconnected from already crystallized regions (this behavior is seen in Figure 3a,b and then in Figure 3d−h in the bottom right-hand corner of the images) and growth that occurs essentially radially from the initial crystallization, crossing many cylinder boundaries, in which the crystalline region is continuous and the growth front can be followed. From examination of these and other similar data sets, we find that only the second type of growth is found in the late stages of crystallization. In experiments on homopolymers we have found similar behavior in that in the early stages of crystallization disconnected lamellae appear in an area, and then later growth occurs continuously and radially from this site. Considering the thickness of the films, we suggest that initially nucleation occurs somewhere below the sample surface and growth occurs until the crystallites impinge with the sample surface—this is responsible for the first type of behavior. Subsequently growth occurs radially in a manner more similar to that seen in the bulk, although in the current case the constraint that the surface applies to the mesophase (i.e., the probable existence of a surface layer of uncrystallizable material and the subsequent alignment of the cylinders in the plane of the surface) will influence the crystallization behavior.

The topographic images, Figure 3i−l, show the phase-separated melt structure with a height change between phases of 0.5−1 nm, although once crystallization has progressed the data become more indistinct. Topographic images obtained with AFM can be prone to artifacts if there are variations in the material properties of the surface being imaged. The topographic variations indicating the melt structure in block copolymers are believed to be a result of such an artifact, either because of the increased penetration of one phase by the probe due to the difference in stiffness between the two phases or, in the case where there are differences in adhesive forces or in long-range attractive forces (e.g., electrostatic, hydrophobic/hydrophilic etc.), because of a more complicated interaction with the oscillating probe.[20] The change in height that occurs during crystallization is minimal. Individual crystallites, such as those growing toward the top right of Figure 3k, typically protrude between 0.5 and 1 nm above the level of the surrounding melt. Again, it is possible that this apparent height difference is an artifact caused by the difference in stiffness between the crystal and melt phases. The total height change during crystallization of less than 10 nm is less than would typically be observed in a comparable homopolymer crystallization experiment. Supporting Information S2 is a movie showing the full sequence of phase images collected during this experiment.

Figure 4 shows the rates of growth of 12 of the crystallites shown in Figure 3, measured between consecutive images, all

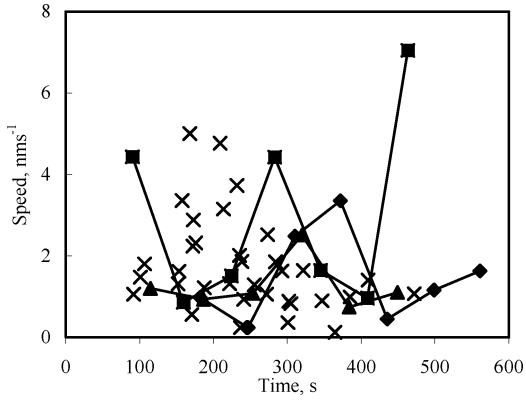

Figure 4. Graph showing the growth rates of 12 of the crystallites shown in Figure 3. Growth rates were measured between consecutive frames. ■ is the crystallite labeled A, ◆ is the crystallite labeled B, and ▲ is the crystallite labeled C. The crosses are growth rates measured at different times for the other nine crystallites. The growth rates of these three crystallites are tracked for clarity—joining all of the growth rates in a similar manner produces a confusing graph. These three crystallites are typical in the amount that their rates vary.

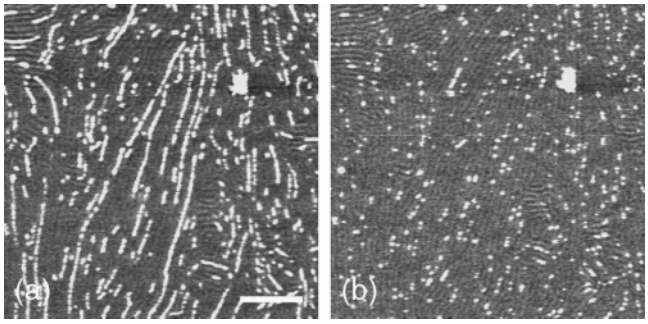

Figure 5. Two AFM phase images showing the melting of E/MB: (a) taken at 113.2 °C; (b) taken at 115 °C, 316 s after (a). Black to white represents a change in phase of 2°. The scale bar represents 1 μm.

of which are of the "radial" growth type described above. The rates of three crystals (A, B, and C in Figure 3) are highlighted by denoting their rates with different symbols and joining them with a line, from which it can be seen that the rates vary with time for each crystal as well as between crystals, with an overall average rate for all 12 crystals of 1.8 nm s^{-1}. The effect of the melt structure on growth rates is complex. Crystals that grow fast tend to travel for significant distances along existing polyethylene cylinders in the melt, as can be seen for instance in the rapid growth of crystal A between images b and c of Figure 3. Also, the direction of growth is sometimes altered by the melt structure, with the crystal changing direction subtly so as to remain within an existing ethylene cylinder (as can be seen for crystal B in images d and e). However, fast growing crystals will also cross multiple E/MB boundaries, for instance the rapid growth of crystal A between images c and d. Replotting the data to show the growth rate against the number of E/MB boundaries crossed does not show any correlation.

During initial growth, it is clear from Figure 3 that there are only minor rearrangements of the melt in front of a growing crystal. The melt structure is essentially constant until just before the crystals impinge on the cylinders shown, when some subtle reorganizations can be seen (examples marked in Figure 3 with arrows).

Following crystallization at 95 °C, the sample was slowly heated to 118 °C. Figure 5 shows the evolution of the crystalline cylinders during the last stages of melting. Melting occurs sporadically along the crystallites, the cylinders breaking up into apparently random segments. It is just possible to discern the structure within the melt, from which it can be seen that there is no rapid reorganization after melting, the more ordered structure that has been laid down during growth remaining on melting.

The E/SEB material crystallizes considerably more slowly than the E/MB and can be quenched to lower temperatures,[3] allowing the growth kinetics to be studied using in situ AFM over a wider temperature range. Figure 6 shows crystallization at 85 °C from the spherical melt. A densely branched "seaweed" structure occurs during growth. The large, static spots on the image are most probably a small fraction of PE homopolymer (terminated first block in the diblock). As the total volume of these "spots" is estimated to be less than 0.01% of the sample (considering the thickness of the films, their surface density, and the height of the spots measured as ~2 nm), such a small concentration of PE homopolymer would not be detectable in the gel permeation chromatography trace.[3] PE has a lower surface energy than SEB, and the PE block is known to wet the surface in E/SEB diblocks.[28] This suggestion is supported by the observation that crystallization crosses these regions instantaneously (within the time resolution of the technique), as expected for PE homopolymer at this supercooling. The "seaweed" structure itself has an unusual appearance, with a bright rim around a darker central region in each of the branches, unlike the structures observed in much thinner films of the same polymer.[28] The corresponding topographic images show a similar appearance, as can be seen from the example in Figure 7, where the accompanying cross section shows the "depth" of the depression in the center of the arm. As the lateral sizes of the depressions are considerably larger than the block size, it is most likely that they are real topographic features in this case.

From Figure 6 it can be seen that there is a preferential branch angle of ~60°. The graph in Figure 8 shows growth rates taken from the series of images shown in Figure 6. There is a wide scatter around an average of 1.6 nm s^{-1}. The time dependence of the growth rate is highlighted for three of the branches, marked "A", "B", and "C" in Figure 6, by joining the points. This is just to guide the reader, as, considering the serial nature of the data collection, it is not clear whether differences in rate occur because of sudden spurts or through a high continuous rate over the period of time between measurements. At 80 °C (data not shown) the average rate of growth was 2.3 nm s^{-1}, again with a broad range of rates from 0.5 to 5.3 nm s^{-1}.

The initial fingering growth in the sphere-forming E/SEB leaves a substantial fraction of the material between the fingers uncrystallized. Figure 9a−c is a higher magnification series of images showing the gradual incorporation of all of the crystallizable material at 85 °C. These images were taken of the growth tip of the same structure shown in Figure 6. Supporting Information S3 is a movie showing the full sequence of images collected during this experiment. From these images the low level of order within the melt is clear. Initial growth is rapid and proceeds primarily vertically down the images with branching continuing primarily on the right-hand side, as in Figure 6. The left-hand side of the crystal growing in the center of the image does not branch during this initial stage, but the slow formation of a finer branching texture can be seen to develop which does appear to follow the nearest-neighbor direction in the surrounding melt. Growth of this structure is slow and is eventually overtaken by the arrival and rapid growth of another primary arm.

Figure 9d−f shows a series of images taken during crystallization at 75 °C. At this temperature the templating of the

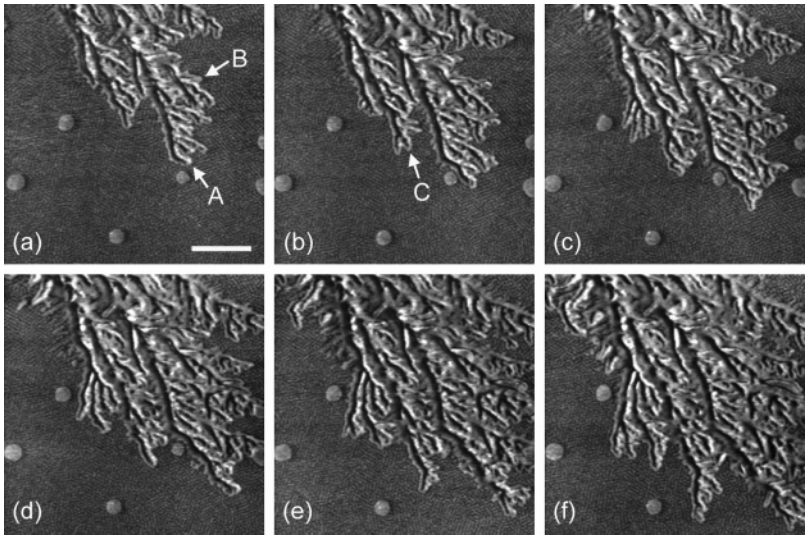

Figure 6. A series of AFM phase images showing the crystallization of E/SEB at 85 °C. A, B, and C indicate crystallites referred to in the text. (a) Taken at 0 s, (b) at 102 s, (c) at 205 s, (d) at 307 s, (e) at 409 s, and (f) at 512 s, each image collected in 51 s. Black to white represents a change in phase of 20°. The scale bar represents 500 nm.

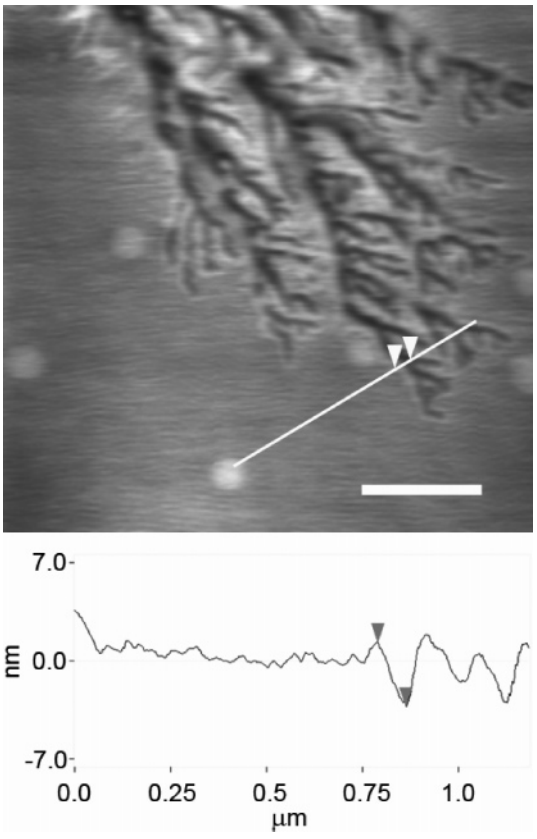

Figure 7. AFM topographic image collected simultaneously with Figure 6c. The line shows the region over which the line profile, given below, was taken, the arrows in the image marking the points denoted by arrows in the profile. Black to white represents a change in height of 15 nm. The scale bar represents 500 nm.

branched seaweed structure is much clearer, with branch angles of 70° and 90° predominating. At this lower temperature the arm width is considerably reduced and correlates with the intersphere separation. We were not able to capture the growth of the primary front, but only the growth of sidearms. The combination of a higher nucleation density and a high rate makes in-situ observation problematic. The average growth rate of the sidearms is 1.9 nm s^{-1}, slower than that measured 5 °C hotter (2.3 nm s^{-1} at 80 °C). However, the lowest growth rates

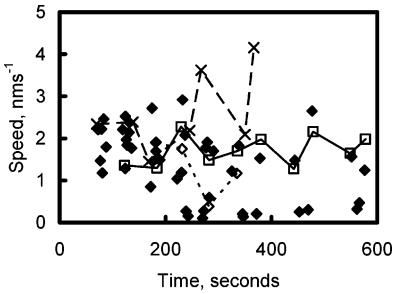

Figure 8. Graph showing the rates of growth of 14 of the growth tips shown in Figure 6. Growth rates were measured between consecutive frames. × is the crystallite labeled A, □ is the crystallite labeled B, and ◇ is the crystallite labeled C. The growth rates of these three crystallites are tracked for clarity—joining all of the growth rates in a similar manner produces a confusing graph. These three crystallites are typical in the amount that their rates vary. The black diamonds show the growth rates measured at different times of the other 11 crystallites.

measured were close to the average, so it is likely that, as the primary front could not be imaged, the distribution is slanted toward the slow end.

Discussion

The aim of this study was to gain a better understanding of how break-out crystallization occurs in block copolymers at the single domain level and to use block copolymer crystallization to obtain insights into polymer crystallization in general. In the following we will discuss the crystallization from each of the different melt structures in turn, while referring to these two aims.

Crystallization from the Cylindrical Melt. It is immediately apparent that the process of crystallization has remarkably little impact on the melt structure right up until the point of crystallization. At high temperatures (130 °C in this study) the melt slowly relaxes toward a more stable structure with the cylinders lying parallel to the surface. A priori, we expected that confined crystallization would leave the melt structure unchanged but that in break-out crystallization the melt would undergo considerable reorganization ahead of the growth front. During any crystallization process from the melt there will be transport of material driven by the volume change that occurs on crystallization—the crystal phase is, typically, more dense

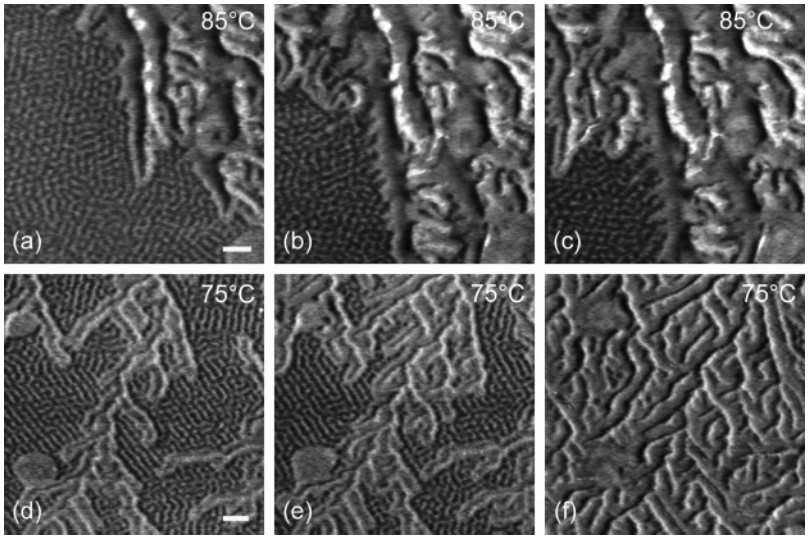

Figure 9. (a−c) A series of AFM phase images showing crystal growth at 85 °C: (a) taken at 0 s, (b) taken at 342 s, and (c) taken at 508 s, each image collected in 42 s. Black to white represents a change in phase of 20°. The scale bar represents 100 nm. (d−f) A series of AFM phase images showing crystal growth at 75 °C: (d) taken at 0 s, (e) taken at 63 s, and (f) taken at 503 s, each image collected in 63 s. Black to white represents a change in phase of 20°. The scale bar represents 100 nm.

than the amorphous phase. In the bulk the volume change will lead to a depletion layer (i.e., a region of lower density melt) immediately adjacent to the growth front, which can be relieved either rapidly by flow of material or more gradually through diffusion. The issue of negative pressures occurring during polymer crystal growth has been discussed in detail in the literature.[29] Additionally, in phase-separated block copolymers, when crystallization is occurring through breakout and ethylene−MB boundaries are being crossed, there must also be transport of ethylene blocks across the boundary. The presence of structure within the melt that can be imaged with the AFM provides a mechanical "label" for the location of the different molecular species, and it might be expected that any motion of the melt would cause a distortion of the imaged structure.

Examination of the images shows very little sign of distortion of the melt by the growing crystals. The examples indicated in Figure 3, where rearrangement does occur, appear to be evidence of a relaxation after crystallization. When an ethylene crystal crosses at right angles to an ethylene domain, it is still necessary for MB blocks to be adjacent to the crystal along its entire length due to the connectivity between the units. This means that ethylene units that have not been incorporated into the crystal need to reorganize to maintain the phase-separated domain structure. Apparently, the rate of crystal growth is considerably faster than the rate of domain reorganization so there is no large-scale relaxation of the domain structure to accommodate the local increase in defects induced by crystallization. Transport of material occurs across microdomain boundaries, without detectable changes in the boundary or the local composition, and does not redefine the orientation and position of the microdomains. This implies that diffusion, rather than flow, is the main mechanism. However, there is no evidence that this diffusive process is the main barrier to growth in the cylinder forming materials—a combination of surface (e.g., nucleation) and transport processes is most likely responsible for the growth rate, as in homopolymers.

Two contrasting growth behaviors are seen, with growth from below the surface apparently resulting in the melt cylinders strongly controlling the growth direction, while growth along the surface leads to little impact of the melt structure on growth direction. It is likely that the second behavior is the most common behavior within the bulk of the sample at this small undercooling. When the cylinders reach the sample surface, they can no longer continue to grow along their existing trajectory and must branch if growth is going to continue. The most likely direction for this branch to occur is along an existing melt cylinder, as that is the area where the transport barrier to crystal growth is smallest.

The growth rates measured on the example shown here, and on other examples, reveal a complex behavior. Observation of isolated cases shows clearly that when the most rapid growth occurs, it does so along an existing melt cylinder. However, analysis of the growth rate of a large number of crystals does not show the expected inverse correlation between growth rate and the number of ethylene−MB boundaries crossed. Examination of individual growing crystallites reveals that in many cases a crystal will get stuck at a boundary for several minutes, while at another stage of growth it will rapidly cross apparently similar boundary geometries. As a crystal crosses an E−MB boundary there will be an energy penalty due to the formation of a new interface with high curvature. The extent to which this can relax will depend on the local structure in the surrounding phase separated melt, over a length scale of several hundred nanometers, as well as on the presence and growth of other crystals within this volume. From inspection of the images, it appears that the melt structure changes subtly so as to allow either an orthogonal or parallel alignment of the melt structure with the crystallites; acute angles between the crystal growth direction and the cylinder axes are not observed, as noted previously from TEM examination of fully crystallized specimens.[3] The present AFM observations reveal the origin of this behavior: growth of a crystallite at an acute angle relative to the cylinder axis would suffer a greater energetic penalty than growth at a right angle, due to the larger area of new interface created by the crystal. To predict the ease with which a boundary will be crossed will require an assessment of the ability of the melt to locally reorganize as well as similar contributions from the (unobserved) melt below the sample surface. To unambiguously quantitatively assess the impact of the melt on the growing crystals, it will be necessary to look at films that are a single domain thick—such a study is beyond the scope of the current work.

In summary, the extent to which growth is templated by the cylinders in this E/MB diblock is rather limited at these small

supercoolings, in line with the extrapolation of previous experiments,[22,30] in which decreasing supercooling showed a transition from complete confinement (on rapid cooling) to less confinement (on crystallization at 77 °C). Growth occurs in a particular direction (essentially radially from the initial nucleation site) with only limited branching, and if a growing crystal happens to enter an ethylene-rich cylinder parallel to its growth direction, its growth rate will increase, but the direction of growth is not substantially influenced by the existing melt structure.

The driving force for crystallization is clearly substantially greater than that for phase separation (considering the difference in heat associated with the two transformations—of order 100 J/g for polyethylene homopolymer crystallization compared to order 1 J/g for a block copolymer order−disorder transition[31]), so it is perhaps not surprising that, when both phases are mobile, crystallization dominates. However, it should be stressed that thermodynamics does not require the destruction of the preexisting melt-structure—as pointed out in ref 3, the relatively low crystallinity of the hydrogenated polybutadiene "polyethylene" means that the total crystallinity obtainable within microdomains is the same as that obtained on breakout. But by studying the phase transformation as it happens, we are led to additional factors contributing to the total free energy that may differ between confined and free growth. Following the preparation route we have used, the melt phase consists of cylinders with a short persistence length (which coarsens only slowly with time[14]), and for a crystal to grow within such tortuous cylinders would require a high degree of curvature, introducing an energy penalty. Second, as discussed above, there is the penalty associated with the structure of the melt phase adjacent to the crystal that drives the melt toward perpendicular or parallel alignment to the growing crystal. Combined these will tend to favor break-out crystallization with some reorganization of the melt either during or after growth. The final factor, though, is kinetic—diffusion of E blocks to the growing crystal face is most rapid if the diffusion occurs along the cylinder axis, as this does not require movement of the entire block copolymer chain. It is this that leads to the more rapid growth that is seen when chance leads to the alignment of a growing crystal parallel to an existing ethylene-rich domain.

On melting, the cylindrical crystals break up into small blocks. In these materials, the crystallites are very small laterally. In polyethylene homopolymer we have observed that melting of lamellae occurs back from the lamellar edges but does not tend to lead to the breaking of crystals into small pieces.[32] However, here, as the crystals are of needlelike aspect, rather than platelike, it is not surprising that a similar process of melting from local defects at edges will lead to the crystallites breaking up into small pieces. The melt is left with large oriented grains that reflect the crystal morphology that had grown at lower temperature; i.e., the melt structure retains the local orientation that is imposed by crystallization.

Crystallization from the Spherical Melt. The morphology during crystallization from the spherical melt is markedly different from that seen for the cylindrical melt and from homopolymers. The "seaweed" structure is a typical diffusion-limited growth pattern[33] and implies that the morphology is controlled by the diffusion of ethylene blocks across SEB domains toward the growth front. In homopolymer crystallization transport of material is driven by the need to replace material that has been incorporated in the crystal, while here that material will instead be replaced by noncrystallizable material and needs to be exchanged through a diffusive process with crystallizable ethylene units. The occurrence of this diffusion-controlled morphology is in contrast to the behavior seen in the cylinder-forming material.

Considering the low concentration of polyethylene, it is not surprising to see a diffusion-controlled process at these relatively high supercoolings. What is new is the structure within the melt that adds a direction to the diffusion. There are many different types of diffusion-limited growth patterns, and the seaweed structures here, characterized by frequent tip splitting, are most commonly associated with a low level of surface tension anisotropy. The occurrence of this morphology is surprising as the ordered melt might be expected to introduce an effective anisotropy, in analogy with experiments on diffusive processes using Hele−Shaw cells[34] in which the introduction of anisotropy in the available diffusive paths has been shown to play a similar role to an anisotropic surface tension. The apparent contradiction most likely occurs because of the connectivity of the crystallizable and noncrystallizable units. This places a limit on the maximum size of the growing crystals, forcing tip splitting over the same length scale as the underlying melt structure. We do see a clear dominance of branches along angles that are close to the nearest-neighbor angles in the melt structure, showing that, as expected, diffusion occurs more rapidly in these directions, as they are the ones along which the minimum length of SEB matrix must be traversed by a diffusing E block. As the material is cooled, the templating of the crystal structure by the melt increases. There is an increase in the degree of melt segregation, and an increase in driving force for crystallization, and hence growth rate relative to the rate of diffusion. Both factors are expected to lead to an increased level of templating.[3] At lower temperatures we see a range of preferred branch angles from 70° to 90°, but with all the branches now having a high angle similar to that of the nearest-neighbor angle in the melt.

From the AFM images it is not possible to tell what the crystallographic relationship between the different parts of the seaweed structures is. Dendrites are often single crystals, and it might be expected that in a two-dimensional densely branched or seaweed structure such as those observed here, crystallographic registry between the branches would be maintained. In this case, the morphology observed would be the equivalent of a single lamella in a conventional polymer, broken up because of the surface instability and maintaining a texture after growth is completed because of the presence of the noncrystallizable block. Alternatively, the branching could be noncrystallographic (so more similar to lamellar branching in a spherulite). Unfortunately, it is not possible to discern between these alternatives by AFM, while other techniques, such as electron diffraction, cannot be applied in this case where the "crystal" of interest is a thin layer at the surface of a relatively thick film.

The measurements of growth kinetics are again hindered by the serial nature of the data collection and the still relatively fast growth rates. We were not able to obtain good data during crystallization at the lowest temperatures where templating was strongest, nor could we obtain sufficient data to analyze the process of branching and its effect on rates or the shape of the growth tip prior to branching.[35] What we do see is that the growth is sporadic on the length and time scales that we were accessing, with some branches growing consistently slower or faster than the average, but still with a fluctuating rate. We did not find any clear correlation between these variations in growth rate and the relative location of the growth tip being measured. In many diffusion-controlled growth processes a steady-state growth rate is reached for the advancing growth tip. However,

in the situation here the length scale over which we are measuring the growth rate (around 100 nm) is comparable to the length scale over which the diffusion rate will vary (the length scale of the spherical domains, about 30 nm), so the observed variations in growth rate are expected.

At the highest supercooling observed we were not able to capture images during the most rapid growth period, so the data are not representative. However, the increase in average crystal growth rate from 1.6 to 2.3 nm s^{-1} with a temperature change of 5 °C (85 to 80 °C) is quite comparable to the increase in overall crystallization rate, measured at similar temperatures.[3]

Conclusions

The crystallization behavior of sphere and cylinder forming block copolymers, in which ethylene is the crystallizable unit, has been followed in situ, in real time, using hot-stage AFM. The existence of image contrast between the two melt phases and the crystalline phase allow the effect of the melt structure on the crystallization process to be assessed.

In E/MB, the cylinder-forming system, a coarse, radial structure is formed. Growth occurs faster along existing ethylene-rich cylinders in the melt, but the radial direction of growth dominates. The melt structure is unaltered until impingement by the growing crystals, so crystallizable material is transported to the growth front by diffusion rather than by flow. The rate of relaxation of the melt structure is considerably slower than the rate of crystal growth in this system.

In E/SEB, the sphere-forming system, a densely branched "seaweed" structure is formed, reminiscent of dendritic growth under conditions of low surface tension anisotropy and implying that the morphology is controlled by the diffusion of material across microdomain boundaries. As the crystallization temperature is reduced, crystalline branch angles are increasingly dominated by nearest-neighbor axes within the spherical melt structure, approaching but not reaching the condition of confinement that has been reported at greater supercoolings.[3,5] In this material it was only through direct, in situ observation that the crystallization morphology could be determined.

Acknowledgment. J.K.H. thanks the Engineering and Physical Sciences Research Council, UK, for funding and Prof. M. J. Miles, University of Bristol, for support. R.A.R. gratefully acknowledges support from the U.S. National Science Foundation, Polymers Program (DMR-0220236 and DMR-0505940), as well as Gary R. Marchand, Daniel J. Quiram, and Yueh-Lin Loo for the synthesis and molecular characterization of the block copolymers studied herein.

Supporting Information Available: Three movies (.avi) showing the complete data set corresponding to the individual frames given in the text: S1, cylinder melt microdomain reorganization corresponding to Figure 2; S2, crystallization from the cylindrical mesophase corresponding to Figure 3; S3, crystallization from the spherical mesophase corresponding to Figure 9. This material is available free of charge via the Internet at http://pubs.acs.org.

References and Notes

(1) Rangarajan, P.; Register, R. A.; Fetters, L. J.; Bras, W.; Naylor, S.; Ryan, A. J. *Macromolecules* **1995**, *28*, 4932.
(2) Zhu, L.; Chen, Y.; Zhang, A.; Calhoun, B. H.; Chun, M.; Quirk, R. P.; Cheng, S. Z. D.; Hsiao, B. S.; Yeh, F.; Hashimoto, T. *Phys. Rev. B* **1999**, *14*, 10022.
(3) Loo, Y.-L.; Register, R. A.; Ryan, A. J. *Macromolecules* **2002**, *35*, 2365.
(4) Reiter, G.; Castelein, G.; Sommer, J. U.; Rottele, A.; Thurn-Albrecht, T. *Phys. Rev. Lett.* **2001**, *87*, 226101.
(5) Loo, Y.-L.; Register, R. A.; Ryan, A. J. *Phys. Rev. Lett.* **2000**, *84*, 4120.
(6) Loo, Y.-L.; Register, R. A.; Ryan, A. J.; Dee, G. T. *Macromolecules* **2001**, *34*, 8968.
(7) Hobbs, J. K.; McMaster, T. J.; Miles, M. J.; Barham, P. J. *Polymer* **1998**, *39*, 2437.
(8) Pearce, R.; Vancso, G. J. *Macromolecules* **1997**, *30*, 5843.
(9) Schultz, J. M.; Miles, M. J. *J. Polym. Sci., Part B: Polym. Phys.* **1998**, *36*, 2311.
(10) Li, L.; Chan, C.-M.; Li, J.-X.; Ng, K.-M.; Yeung, K.-L.; Weng, L.-T. *Macromolecules* **1999**, *32*, 8240.
(11) Magonov, S. N.; Yerina, N. A.; Ungar, G.; Reneker, D. H.; Ivanov, D. A. *Macromolecules* **2003**, *36*, 5637.
(12) Pearce, R.; Vancso, G. J. *J. Polym. Sci., Part B: Polym. Phys.* **1998**, *36*, 2643.
(13) Beekmans, L. G. M.; van der Meer, D. W.; Vancso, G. J. *Polymer* **2002**, *4*, 1887.
(14) Harrison, C.; Adamson, D. H.; Cheng, Z. D.; Sebastian, J. M.; Sethuraman, S.; Huse, D. A.; Register, R. A.; Chaikin, P. M. *Science* **2000**, *290*, 1558.
(15) Knoll, A.; Lyakhova, K. S.; Horvat, A.; Krausch, G.; Sevink, G. J. A.; Zvelindovsky, A. V.; Magerle, R. *Nat. Mater.* **2004**, *3*, 886.
(16) Vasilev, C. Ph.D. Thesis, Organisation et cristallisation des copolymères blocs en couches minces (or, in English, Ordering and crystallization of block copolymers in thin films), Université de Haute Alsace, 2004, library no. 20004127.
(17) Quiram, D. J.; Register, R. A.; Marchand, G. R. *Macromolecules* **1997**, *30*, 4551.
(18) Hobbs, J. K.; Humphris, A. D. L.; Miles, M. J. In *Applications of Scanned Probe Microscopy to Polymers*; ACS Symposium Series 897; Batteas, J. D., Michaels, C. A., Walker, G. C., Eds.; Oxford University Press: Oxford, 2005; p 194.
(19) Hobbs, J. K.; Humphris, A. D. L.; Miles, M. J. *Macromolecules* **2001**, *34*, 5508.
(20) Cleveland, J. P.; Anczykowski, B.; Schmid, A. E.; Elings, V. B. *Appl. Phys. Lett.* **1998**, *72*, 2613.
(21) Fetters, L. J.; Lohse, D. J.; Richter, D.; Witten, T. A.; Zirkel, A. *Macromolecules* **1994**, *27*, 4639.
(22) Tierney, N. K.; Register, R. A. *Macromolecules* **2003**, *36*, 1170.
(23) Krishnamoorti, R. K.; Graessley, W. W.; Balsara, N. P.; Lohse, D. J. *Macromolecules* **1994**, *27*, 3073.
(24) Graessley, W. W.; Krishnamoorti, R. K.; Reichart, G. C.; Balsara, N. P.; Fetters, L. J.; Lohse, D. J. *Macromolecules* **1995**, *28*, 1260.
(25) Quiram, D. J.; Register, R. A.; Marchand, G. R.; Adamson, D. H. *Macromolecules* **1998**, *31*, 4891.
(26) Segalman, R. A.; Yokoyama, H.; Kramer, E. J. *Adv. Mater.* **2001**, *13*, 1152.
(27) Angelescu, D. E.; Waller, J. H.; Register, R. A.; Chaikin, P. M. *Adv. Mater.* **2005**, *17*, 1878.
(28) Li, Y.; Loo, Y.-L.; Register, R. A.; Green, P. F. *Macromolecules* **2005**, *38*, 7745.
(29) Galeski, A.; Koenczoel, L.; Piorkowska, E.; Baer, E. *Nature (London)* **1987**, *325*, 40.
(30) Quiram, D. J. Ph.D. Thesis, Princeton University, 1997.
(31) Loo, Y.-L.; Register, R. A. In *Developments in Block Copolymer Science and Technology*; Hamley, I. W., Ed.; Wiley: Chichester, 2004; p 213.
(32) Hobbs, J. K. *Chin. J. Polym. Sci.* **2003**, *21*, 135.
(33) Granasy, L.; Pusztai, T.; Borzsonyi, T.; Warren, J. A.; Douglas, J. F. *Nat. Mater.* **2004**, *3*, 645.
(34) Ben-Jacob, E.; Garik, P.; Mueller, T.; Grier, D. *Phys. Rev. A* **1988**, *38*, 1370.
(35) Utter, B.; Bodenschatz, E. *Phys. Rev. E* **2002**, *66*, 051604.

MA0514020